

Online Research @ Cardiff

This is an Open Access document downloaded from ORCA, Cardiff University's institutional repository: <https://orca.cardiff.ac.uk/id/eprint/115771/>

This is the author's version of a work that was submitted to / accepted for publication.

Citation for final published version:

Zagorscak, Renato ORCID: <https://orcid.org/0000-0002-8408-8585> and Thomas, Hywel Rhys ORCID: <https://orcid.org/0000-0002-3951-0409> 2018. Effects of subcritical and supercritical CO₂ sorption on deformation and failure of high-rank coals. International Journal of Coal Geology 199 , pp. 113-123. 10.1016/j.coal.2018.10.002 file

Publishers page: <http://dx.doi.org/10.1016/j.coal.2018.10.002>
<<http://dx.doi.org/10.1016/j.coal.2018.10.002>>

Please note:

Changes made as a result of publishing processes such as copy-editing, formatting and page numbers may not be reflected in this version. For the definitive version of this publication, please refer to the published source. You are advised to consult the publisher's version if you wish to cite this paper.

This version is being made available in accordance with publisher policies.

See

<http://orca.cf.ac.uk/policies.html> for usage policies. Copyright and moral rights for publications made available in ORCA are retained by the copyright holders.



Effects of subcritical and supercritical CO₂ sorption on deformation and failure of high-rank coals

Renato Zagorščak^{a*} and Hywel Rhys Thomas^a

^a Geoenvironmental Research Centre (GRC), School of Engineering, Cardiff University, The Queen's Buildings, The Parade, Cardiff, CF24 3AA

*corresponding author (ZagorscakR@cardiff.ac.uk)

Abstract:

This paper presents the results of an extensive experimental analysis aimed at establishing the effects of subcritical and supercritical CO₂ sorption on deformation and failure of coals. Two high-rank anthracitic coals from the South Wales coalfield, obtained from different locations and depths of 150 m and 550 m, are employed for that purpose. The investigations include i) determination of unconfined compressive strengths and elastic moduli of the cores both non-saturated and saturated with CO₂ at 2.1 MPa, 4.3 MPa and 8.5 MPa, ii) assessing the dependence of the parameters obtained on CO₂ pressure, iii) analysing the effect of CO₂ saturation on failure patterns of the samples tested and iv) determination of the particle size distribution after the failure of the samples. Based on the results of twenty coal specimens tested, it is demonstrated that CO₂ sorption reduces the uniaxial compressive strengths and elastic moduli by between 29% and 83% for the range of pressures studied. The reductions observed increase gradually up to 4.3 MPa and then reach a plateau. By accommodating the effect of effective stress on compressive strength values, it is shown that chemical weakening of high rank coals is mostly associated with sorption of subcritical CO₂, with negligible impact of supercritical CO₂ on further parameter reduction. Inspection of failure patterns during uniaxial compression suggests that non-saturated coal specimens fail through axial splitting with rapid crack propagation and high outburst of coal pieces while the failure of cores subjected to CO₂ injection occurs through multiple fractures with negligible material outburst. The post-failure analysis demonstrates that CO₂ treated samples disintegrate on smaller particles than non-saturated specimens, as up to 5.6 more CO₂ saturated coal pieces passed through the sieves considered in this study than non-saturated pieces. It is claimed that this study presents novel insights into the geomechanical response of high rank anthracitic coals to high pressure CO₂ injection.

Keywords: Coal, Carbon sequestration, Geomechanics, Strength, Elastic modulus, CO₂ adsorption

1. Introduction

Geological sequestration in unmined coal seams offers a prospect of delivering greenhouse gas emissions reductions and at the same time offsetting the costs of CO₂ capture, transportation and storage as the injection of CO₂ in the coal beds allows the production of a value-added product such as methane (White et al., 2005). In general, numerous studies have shown that coal can hold at least twice the volume of CO₂ as CH₄ (Jones et al., 2004; White et al., 2005). However, coals are a mixture of inorganic minerals and organic material that may be affected during the gas injection and adsorption process (Karacan, 2007; Gathitu et al., 2009). Hence, understanding the response of coal under applied stress and storage conditions is of importance for the integrity and safety of the coal seams targeted for CO₂ sequestration and the overlaying strata. This paper aims to enhance such understanding by presenting the experimental investigation of the effects of sub-critical and supercritical carbon dioxide saturation on high-rank coal failure and elastic deformation under uniaxial compressive stress conditions.

The most favourable coal seams for sequestration are occurring at depths where pressure and temperature may exceed the critical values of CO₂, i.e. 750 m (White et al., 2005). At such depths, high rank coals offer a great prospect of storing CO₂ as the maximum sorption capacity generally increases with coal rank (Li et al., 2011; Busch and Gensterblum, 2010). This is related to the fact that high rank coals predominantly contain micropores which provide most of the surface area where gas can adsorb (White et al., 2005).

To date, most research efforts were focused in investigating the geomechanical behaviour of lignite and bituminous coals predominantly exposed to CO₂ in the sub-critical state (Viète and Ranjith, 2006; Perera et al., 2011; Ranjith and Perera, 2012; Perera, 2013; Perera et al., 2013; Hol et al., 2014; Masoudian et al., 2014; Vishal et al., 2015; Ranathunga et al., 2016a; 2016b). Several studies indicated that CO₂ saturation and induced swelling cause crack initiation and enhancement of the fracture lines along the coal increasing the total pore volume (Larsen, 2004; Liu et al., 2010; Hol et al., 2012; Liu et al., 2015). However, very little is known about how anthracitic coals respond to compression after being treated with CO₂, in particular in the supercritical state.

Hence, the geomechanical response of high-rank anthracitic coals under a range of both subcritical and supercritical CO₂ injection pressures up to 8.5 MPa is investigated and discussed in this paper. The results of uniaxial compressive tests of two sets of coal samples obtained from different depths and locations in the South Wales Coalfield are presented. In

total, eight samples are tested in natural air-dried state without CO₂ saturation. Twelve specimens were exposed to different sub-critical and supercritical CO₂ pressures for two weeks before testing. Based on the stress-strain data obtained, unconfined compressive strengths and elastic moduli are calculated and presented. In addition, the change in the measured parameters with an increase in gas saturation pressure is shown and discussed. The reductions in elastic moduli and unconfined compressive strengths are quantified by applying a fitting curve to the experimentally determined values and obtaining the parameters related to the reduction of deformation properties as a function of gas pressure. Failure patterns of non-saturated and CO₂ saturated specimens of both coals are analysed and discussed, based on the photographs taken before and after the coal failure. The distribution of particle sizes after the failure of the samples is also examined.

2. Methodology

2.1. Samples

Coal blocks were collected from two different coal mines, the East Pit East Opencast Coal Site and the Aberpergwm drift coal mine from depths of 150 m and 550 m, respectively. Both coal mines are located in Wales as a part of the South Wales Coalfield (Fig. 1). Coal extracted from the East Pit East Opencast Coal Site is locally known as Black Diamond while coal from the Aberpergwm mine is from a 9ft seam layer and in the future text they will be referred as BD and AB, respectively. The coal blocks obtained on site were wrapped in cling film and put in plastic bags to minimize the oxidation of the coal surfaces and preserve chemical and physical properties. Upon arrival in the laboratory, the sealed blocks were labelled and stored in the constant room temperature environment.

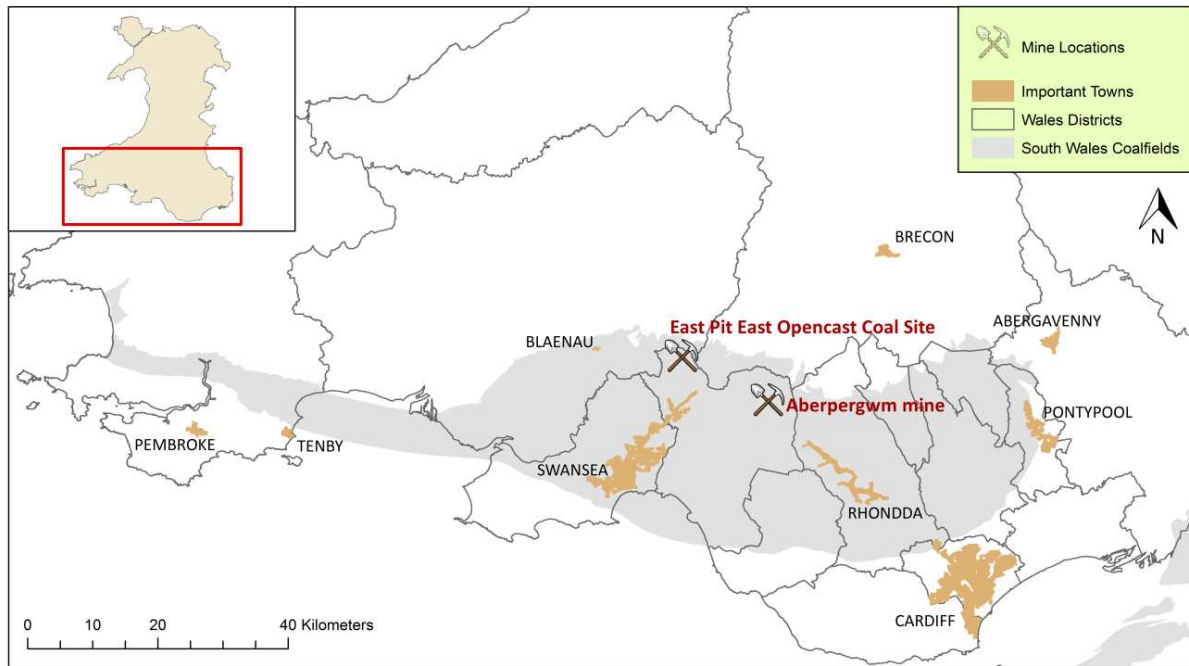


Fig. 1. South Wales Coalfield and locations of the East Pit East Opencast Coal site and the Aberpergwm drift mine.

Coal cores were drilled out of the coal blocks using a coring machine. Water was used as a cooling agent while drilling. Diamond core drilling bit with an internal diameter of 36 mm was used to obtain the coal cores from the Black Diamond and 9ft seam blocks (Fig. 2). Preparation of coal samples for the experiments was conducted following the ASTM D2013/D2013M (2012) standard of practice. As the drying of coal at temperatures higher than 70°C might create new cracks and small fissures leading to alteration of the physical structure of coal (e.g. Gathitu et al., 2009), an air-drying method following the ASTM D3302/D3302M (2015) was applied.



Fig. 2. A typical coal block used for the extraction of coal samples for uniaxial compressive tests.

A total of twenty coal cores were selected for the uniaxial compressive testing. Although a larger number of coal cores has been extracted, only the ones with minimum fractures or small inconsistencies were chosen. The dimensions of the selected samples are shown in Table 1 together with the measured values of mass and density for each core. The average densities of both BD and AB samples are the same, i.e. 1376 kg/m^3 .

Crushed samples passed through a sieve size of 0.212 mm were used for the Proximate and Ultimate analyses, and the results are presented in Table 2. Proximate analysis was performed in accordance to British Standard (BS 1016-104.3, 1998; BS 1016-104.4, 1998; BS 1016-104.1, 1999), while the Ultimate analysis was conducted following the BS 1016-106.1.1 (1996) and BS 1016-106.4.2 (1996). Both BD and AB coals contain high percentage of fixed carbon content, i.e. 90.9% and 88.7%, respectively. Moisture contents, ash contents and volatile matter contents for both samples are relatively low, i.e. 1.65%, 1.65%, 5.82% for BD coal and 0.91%, 4.62%, 5.73% for AB coal, respectively. Based on the results obtained and the comparison with

the ASTM D388 (2015) classification of coal rank, both BD and AB coals can be classified as high rank anthracitic coals.

Table 1

Dimensions and physical properties of core samples used in the uniaxial compressive tests.

Sample	Diameter (cm)	Length (cm)	L/D ratio	Mass (g)	Density (g/cm ³)
<i>Black Diamond</i>					
BD1	3.6	7.6	2.1	107.4	1.376
BD2	3.6	7.6	2.1	107.5	1.376
BD3	3.6	7.7	2.1	108.4	1.373
BD4	3.6	7.6	2.1	108.3	1.378
BD5	3.6	7.5	2.1	106.5	1.377
BD6	3.6	7.5	2.1	106.2	1.377
BD7	3.6	7.3	2.0	103.1	1.374
BD8	3.6	7.1	2.0	101.0	1.378
BD9	3.6	7.4	2.1	104.6	1.370
BD10	3.6	7.2	2.0	101.7	1.380
Average	3.6	7.5	2.1	105.4	1.376±0.003
<i>9ft Aberpergwm</i>					
AB1	3.6	7.5	2.1	108.3	1.391
AB2	3.6	6.9	1.9	98.5	1.376
AB3	3.6	6.8	1.9	96.5	1.376
AB4	3.6	7.9	2.2	113.3	1.389
AB5	3.6	5.6	1.6	78.9	1.367
AB6	3.6	5.6	1.6	80.2	1.392
AB7	3.6	6.0	1.7	83.9	1.364
AB8	3.6	6.4	1.8	89.4	1.365
AB9	3.6	5.3	1.5	74.7	1.365
AB10	3.6	7.5	2.1	106.7	1.379
Average	3.6	6.6	1.8	93.0	1.376±0.011

124

Table 2

Results of the Proximate and Ultimate Analyses.

Characterization test	Black Diamond	9ft Seam
<i>Proximate analysis</i>		
Moisture content, %	1.65±0.12	0.91±0.3
Ash content, %	1.65±0.38	4.62±0.3
Volatile matter, %	5.82±0.21	5.73±0.08
Fixed carbon content, %	90.88	88.73
<i>Ultimate analysis</i>		
Total carbon content, %	90.12±0.11	89.5±0.66
Total sulphur content, %	0.95±0.02	0.87±0.04

2.2. Experimental procedure

In total, twenty coal specimens were tested via an unconfined uniaxial compressive test. Four natural (non-saturated) specimens from each coal seam (BD and AB) were analysed without CO₂ saturation. Six specimens from each coal seam were saturated with CO₂ at designated pressures before uniaxial compression.

Saturation of samples with carbon dioxide was performed in a manometric sorption cell, manufactured by GDS Instruments, which has been used as a saturation chamber for this purpose (Fig. 3). The cell can tolerate pressures up to 20 MPa and temperatures up to 338K. The adsorption cell contains two cavities, each with a volume of approximately 150 cm³. Each chamber is fitted with a GDS Instruments pressure transducer measuring up to 32 MPa and with an accuracy of 0.15%. The cell was placed in a stainless steel tank filled with deionised water which was heated to the designated temperature using Thermo Haake temperature controller with an accuracy of ± 0.01 K. A high pressure injection unit consisting of a dual syringe Teledyne Isco 500D pump system was employed to pressurize CO₂ to the required experimental pressures. The capacity of each syringe pump is 507.38 mL with a pressure range between 0.07 – 25.9 MPa and a standard pressure accuracy of 0.5%. Constant temperature of the pumps was achieved using a Huber Pilot One Ministat 125 temperature controller which circulates deionised water contained in the 2.75 L water tank through heating jackets. Syringe pumps were connected to a liquid withdrawal carbon dioxide cylinder with 99.99% purity in which the tube runs down the centre of the pressurised cylinder and draws the liquid up through the valve. Due to possible contaminants within the cylinder, a filter was fitted at the top of the cylinder. Before injecting CO₂, samples and the pipeline had been vacuumed for one hour to remove any trapped air. Buchi vacuum pump with a pressure of -0.09 MPa was used for that purpose. After that, CO₂ was injected at a designated pressure and kept constant for two weeks. The saturation time of two weeks was based on the work of Zagorščak (2017) who demonstrated that this is sufficient time for the CO₂ to adsorb on the intact specimens of the high-rank coals.

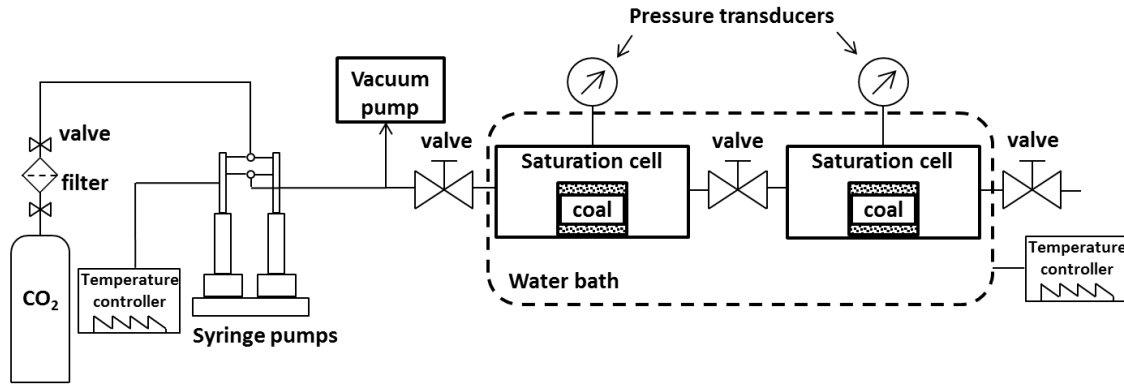


Fig. 3. Schematic of the system used for CO₂ saturation of the samples.

Upon the completion of saturation, chambers were slowly depressurized to avoid any sudden change in pressure which could damage the samples. After removing the specimens from the saturation chamber, they were wrapped in a plastic cling film and tested within a maximum time of one hour.

Uniaxial compressive tests were performed using a Shimadzu Autograph Load Cell AG-I with maximum load capacity of 20 kN. Specimens were placed between top and bottom steel platens. To minimize the impact of a potential unevenness of the sample surface on measured results, two steel blocks were placed between the sample and the top platen. Blocks were able to move with respect to each other when facing uneven surface allowing equal distribution of stress on the coal specimen. Upon sample placement, the axial load on the specimen was then increased and measured continuously.

An attached smart controller showed test force and displacement in real-time, allowing fine position adjustment. Specimens were subjected to a constant loading rate of 0.1 mm/min where the axial displacement of the samples was recorded simultaneously using the built-in displacement transducer of the loading machine. Both the uniaxial compressive strength (UCS) and elastic modulus (E) were calculated following the ASTM D7012 (2014).

2.3. Experimental conditions

Table 3 summarizes the number of specimens and saturation conditions. Results obtained on natural (non-saturated) specimens represent a baseline for all other tests carried out on samples saturated with CO₂ under different saturation conditions.

Table 3

Saturation pressures applied to the coal samples.

Samples	Saturation pressures (MPa)		
	1 st step ~2.1 MPa	2 nd step ~4.3 MPa	3 rd step ~8.5 MPa
<i>Black Diamond</i>			
BD1, BD2, BD3, BD4		No saturation	
BD5	2.12	-	-
BD6	2.12	-	-
BD7	-	4.32	-
BD8	-	4.35	-
BD9	-	-	8.56
BD10	-	-	8.55
<i>9ft Aberpergwm</i>			
AB1, AB2, AB3, AB4		No saturation	
AB5	2.05	-	-
AB6	2.05	-	-
AB7	-	4.25	-
AB8	-	4.25	-
AB9	-	-	8.46
AB10	-	-	8.46

Due to the fact that transition from subcritical to supercritical CO₂ can cause changes in the sorptive potential of CO₂ affecting coal's behaviour (e.g. Perera et al., 2013), temperature of the manometric sorption system was maintained at 313±0.01K (40±0.01°C) enabling carbon dioxide to achieve its supercritical state at high pressures. It should be noted that pressure values mentioned in this study are absolute pressure values calculated assuming the atmospheric pressure of 101 325 Pa. If an average hydrostatic gradient of 0.01 MPa/m and an average thermal gradient of 0.03 K/m (°C/m) with an average surface temperature of 285K (12°C) are assumed (e.g. Gensterblum, 2013), results of this study represent conditions existing up to approximately 900 m of depth.

2.4. Sieve Analysis

In order to get further insights into the post-failure particle size distribution, Black Diamond specimens were analysed immediately after the failure, i.e. four non-saturated specimens and six CO₂ saturated specimens. Sieves with openings of 6.3 mm, 4 mm, 2 mm, 1.18 mm, 0.6 mm and 0.425 mm were used. Calculation of the mass passing through a certain sieve followed a procedure stated in BS 1337-2 (1990).

198 3. Experimental results and analysis

199 Axial stress versus strain curves for non-saturated and CO₂ saturated specimens from Black
200 Diamond and 9ft Aberpergwm coal seams are presented in Fig. 4 and Fig. 5, respectively. By
201 comparing the figures, it can be observed that the stress-strain behaviour of the samples
202 saturated with CO₂ is different than of non-saturated samples. In particular, the samples
203 exposed to CO₂ can be compressed more for the same value of applied stress than the non-
204 saturated samples.

205 Slopes of the curves and maximum recorded stress values of 10 MPa obtained on non-saturated
206 BD specimens are comparable (Fig. 4). The exception is sample BD3 which experienced failure
207 at a lower value of applied stress, i.e. 8 MPa. Fig. 5 shows that the slopes of the curves of non-
208 saturated AB specimens are also comparable, however; maximum recorded stress values range
209 between 5.9 MPa and 9.1 MPa.

210 Experimental results of the two BD specimens saturated with CO₂ at 2.1 MPa show comparable
211 behaviour with maximum recorded stress values of 6.3 MPa (Fig. 4). Although both AB
212 specimens saturated at 2.1 MPa show similar slopes of the curves, maximum stress values are
213 3.6 MPa and 4.6 MPa (Fig. 5).

214 Two BD specimens saturated at 4.3 MPa and two saturated at 8.5 MPa show peak stress values
215 of 2.3 MPa and 1.7 MPa, and 2.9 MPa and 2.4 MPa, respectively (Fig. 4). Similarly, AB
216 samples saturated at 4.3 MPa show maximum stress values of 1.3 MPa and 1.9 MPa, while
217 samples saturated at 8.5 MPa show maximum stresses of 1.5 MPa and 2.1 MPa (Fig. 5).

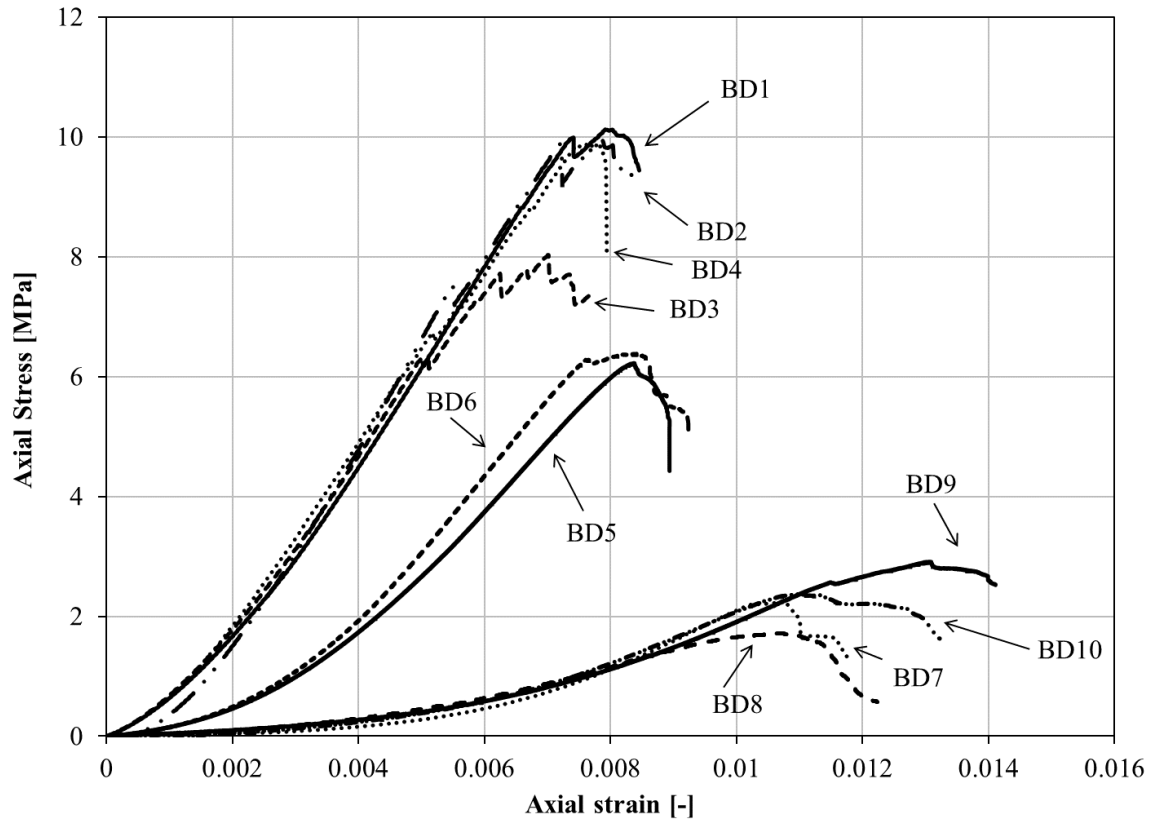


Fig. 4. Axial stress versus strain curves of natural and CO₂-saturated Black Diamond specimens.

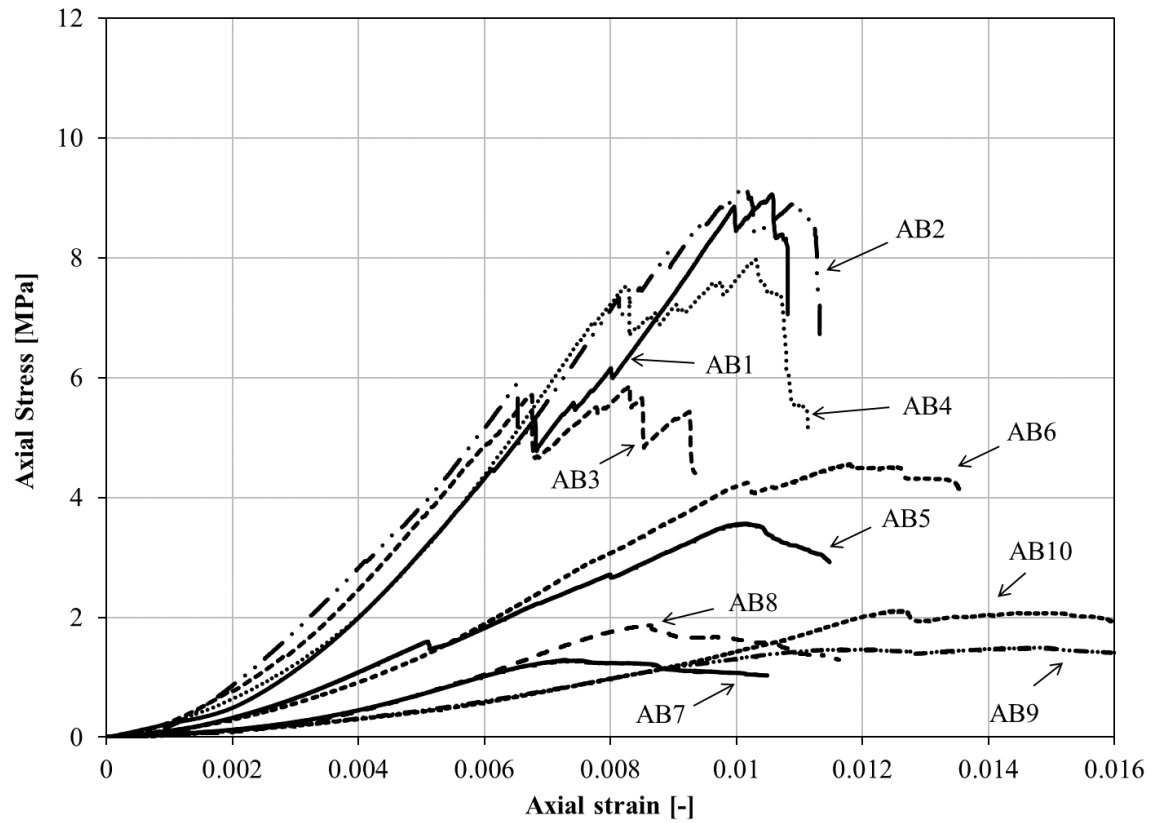


Fig. 5. Axial stress versus strain curves of natural and CO₂-saturated 9ft Aberpergwm specimens.

Calculated values of elastic moduli and unconfined compressive strengths of BD and AB samples are presented in Table 4. Based on the unconfined compressive strengths and elastic moduli of non-saturated specimens and samples saturated at different pressures of each coal, average values are also calculated and presented. In addition, reductions of average values of CO₂-saturated samples with respect to the average values of non-saturated samples are shown. The relationship between the average elastic modulus of non-saturated samples and CO₂-saturated samples used to calculate the reductions presented in Table 4 is:

$$\Delta E = \left(1 - \frac{E_{CO_2}}{E_{natural}}\right) \times 100 \quad (1)$$

where ΔE is the reduction in elastic modulus, $E_{natural}$ (GPa) and E_{CO_2} (GPa) are the elastic moduli of natural (non-saturated) and CO₂-saturated specimens, respectively.

Similarly, reduction in unconfined compressive strength (ΔUCS) is expressed as:

$$\Delta UCS = \left(1 - \frac{UCS_{CO_2}}{UCS_{natural}}\right) \times 100 \quad (2)$$

where $UCS_{natural}$ (MPa) and UCS_{CO_2} (MPa) are the unconfined compressive strengths of natural (non-saturated) and CO₂-saturated samples, respectively.

Table 4.

Unconfined compressive strengths and elastic moduli of natural (non-saturated) and CO₂-saturated Black Diamond and 9ft Aberpergwm coal samples.

Specimen	L/D ratio	UCS (MPa)	Average UCS (MPa)	ΔUCS (%)	E (GPa)	Average E (GPa)	ΔE (%)
Black Diamond							
<i>Natural (non-saturated)</i>							
BD1	2.1	10.12	9.51 ±0.86	-	1.51	1.59 ±0.08	-
BD2	2.1	9.97			1.72		
BD3	2.1	8.03			1.53		
BD4	2.1	9.90			1.57		
<i>2.1 MPa saturated</i>							
BD5	2.1	6.23	6.31	-33.7	1.04	1.13	-29.0
BD6	2.1	6.38	±0.08		1.21	±0.08	
<i>4.3 MPa saturated</i>							
BD7	2.0	2.26	1.99	-79.1	0.48	0.37	-76.8
BD8	2.0	1.72	±0.27		0.26	±0.11	
<i>8.5 MPa saturated</i>							
BD9	2.1	2.91	2.65	-72.2	0.39	0.40	-74.8
BD10	2.0	2.38	±0.27		0.42	±0.02	

9ft Aberpergwm*Natural (non-saturated)*

AB1	2.1	9.06			1.15		
AB2	1.9	9.15	8.01	-	1.06	1.13	-
AB3	1.9	5.86	±1.33		1.15	±0.04	
AB4	2.2	7.97			1.16		

2.1 MPa saturated

AB5	1.6	3.57	4.06	-49.3	0.41	0.49	-56.3
AB6	1.6	4.56	±0.49		0.58	±0.08	

4.3 MPa saturated

AB7	1.6	1.29	1.58	-80.3	0.28	0.29	-74.5
AB8	1.8	1.87	±0.29		0.30	±0.01	

8.5 MPa saturated

AB9	1.5	1.50	1.80	-77.5	0.18	0.19	-82.9
AB10	2.1	2.11	±0.31		0.21	±0.02	

238

239 It can be seen from Table 4 that the average elastic moduli of non-saturated BD and AB
240 specimens are 1.59 GPa and 1.13 GPa, respectively. BD specimens saturated with CO₂ at 2.1
241 MPa, 4.3 MPa and 8.5 MPa exhibit the average elastic moduli of 1.13 GPa, 0.37 GPa and 0.4
242 GPa, respectively. The average elastic moduli of AB specimens saturated with CO₂ at 2.1 MPa,
243 4.3 MPa and 8.5 MPa pressures are 0.49 GPa, 0.29 GPa and 0.19 GPa, respectively.

244 In order to establish a relationship between the measured parameters of all samples, unconfined
245 compressive strengths versus elastic moduli of all tested specimens are plotted in Fig. 6. Elastic
246 modulus and unconfined compressive strength show linear relationship, i.e. samples with
247 higher strength show higher values of elastic modulus.

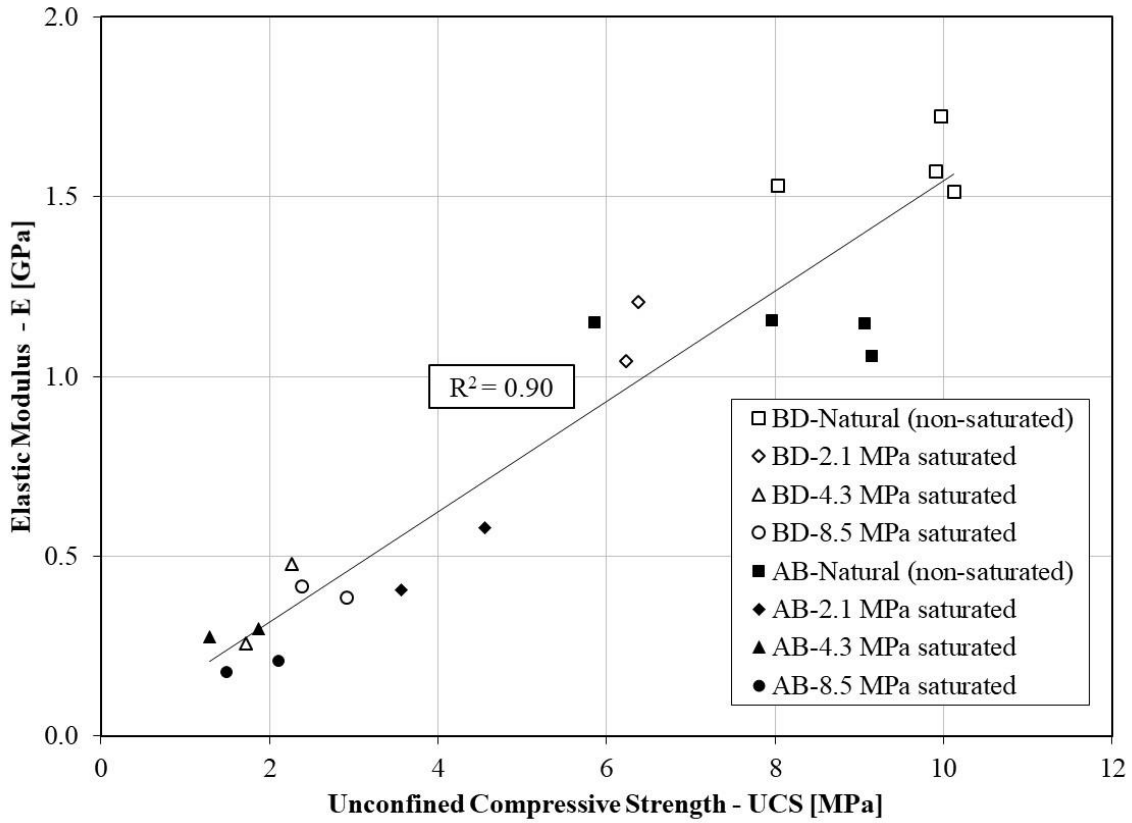


Fig. 6. Uniaxial compressive strengths vs elastic moduli of natural (non-saturated) and CO₂-saturated coal specimens.

Average values of reduction of measured parameters of both coals versus the gas pressure are plotted in Fig. 7. A deviation of parameters between the coals saturated at 2.1 MPa can be observed. In particular, BD samples experienced 29% average reduction in elastic modulus and 34% average reduction in compressive strength. AB samples showed 49% and 56% average reductions in compressive strength and elastic modulus, respectively. As mentioned earlier, Perera et al. (2011) and Ranathunga et al. (2016a) conducted a deformation analysis on lignite coals saturated with CO₂ at 2.1 MPa and 2.0 pressure, respectively. Hence, by comparing the reduction values of samples saturated with CO₂ at 2.1 MPa in this study (i.e. reductions between 29% and 56%) to the reduction values reported in the literature by Perera et al. (2011), i.e. 7-19%, and Ranathunga et al. (2016a), i.e. 6-16%, it can be concluded that saturation of anthracite coal with CO₂ has a more detrimental effect on the measured parameters than of lignite coal subjected to CO₂ at the same pressure. Also, the reduction of parameters measured in this study at 8.5 MPa (72-83%) is greater than the one reported by Ranathunga et al. (2016a) for lignite (40-58%) saturated at 8 MPa, however comparable to the result reported by Perera et al. (2013) for bituminous coal (71-79%) saturated at 8 MPa.

By observing the shape of the curve presented in Fig. 7, it can be inferred that the calculated reductions in measured parameters increase gradually up to 80% at 4.3 MPa and then reach a plateau. Such findings for high rank anthracitic coals are different from the work of Perera et al. (2013) and Ranathunga et al. (2016a) who reported that bituminous and lignite coals exhibit a sudden reduction in mechanical parameters during the transition from subcritical CO₂ at 6 MPa to supercritical CO₂ at 8 MPa.

This might be related to the difference in sorption behaviour of low ranks coals compared to high ranks coals. Siemons and Busch (2007) and Gensterblum et al. (2010) have shown that low rank coals exhibit half of their sorption at higher pressures (e.g. 3.77 MPa) while high rank coals show the opposite behaviour, i.e. half of the sorption is reached at lower pressures (e.g. 0.96 MPa). Similar observation was made by Zagorščak (2017) where BD and AB cores exhibited half of their maximum sorption at pressures lower than 1 MPa. Consequently, it can be expected that majority of structural re-arrangement and its effect on coal strength and elastic modulus occurred in the subcritical region, up to 4.3 MPa in this case, whereas no significant change has been observed with further increase in gas pressure.

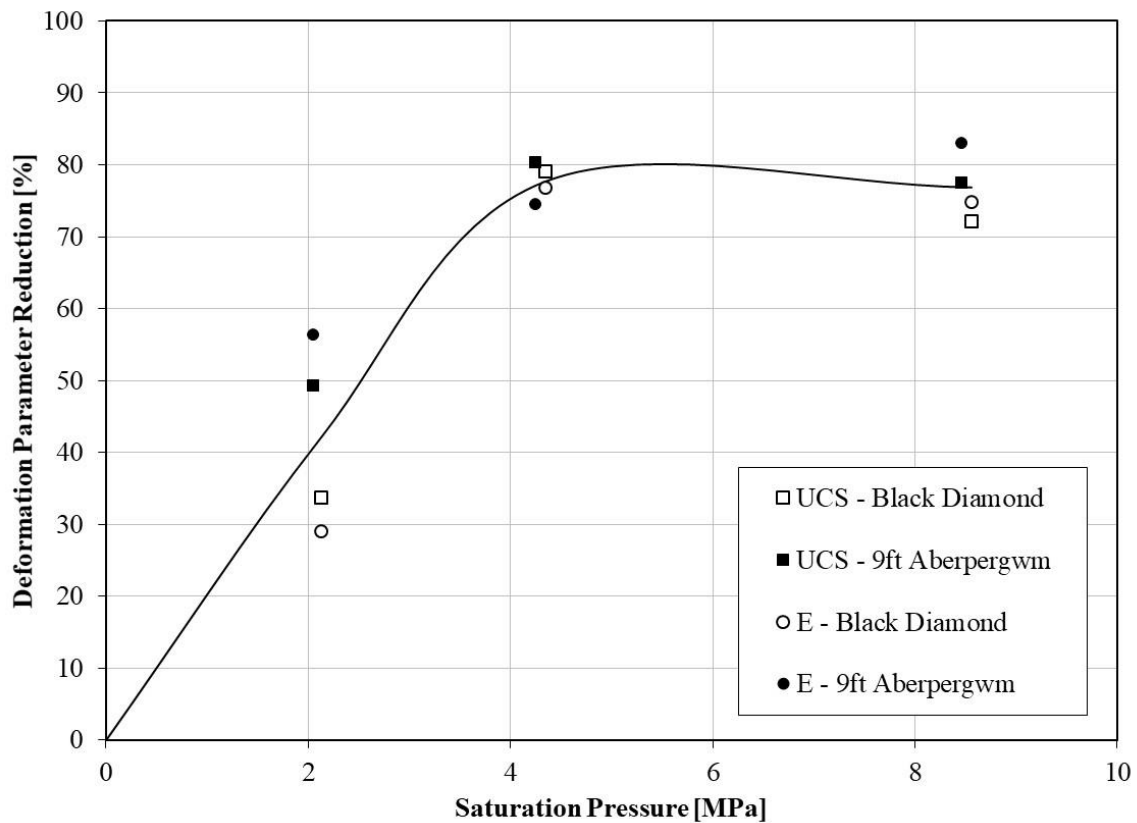


Fig. 7. Reduction of deformation parameters with an increase in CO₂ saturation pressure.

It has been previously suggested that coal samples subjected to sorbing gas are weakened through reduction of effective stress and the internal gas energy release (Wang et al., 2013). Hence, in order to get further insight into the effect of CO₂ sorption and try to distinguish between the effect of effective stress and the alteration of coal structure induced by CO₂ sorption on the strength reduction, both the effective and the residual unconfined compressive strengths versus the saturation pressures are presented in Fig. 8. The effective unconfined compressive strength values were calculated by subtracting the saturation pressures from the unconfined compressive strength determined on samples not saturated with CO₂. It should be noted that during the uniaxial compressive testing, the gas pressure in the samples was not measured. However, it was assumed that due to slow sorption of the CO₂, especially in its subcritical state, on the microporous matrix of the high rank coals and testing the samples within one hour of being removed from the saturation chamber (Zagorščak, 2017), the pressure inside each coal sample remained close to the saturation pressure. Hence, the saturation pressure, which represents the maximum limit to the potential pressure in the fractures, was taken for calculation of the effective unconfined compressive strength. The residual unconfined compressive strength values represent the average strength values measured on samples saturated with CO₂ at different pressures.

Since compressive strengths should index with effective stresses (Wang et al., 2013), Fig. 8 suggests that at sorption pressures of 2.1 MPa and 4.3 MPa, the compressive strengths are reduced by more than the applied saturation pressure. This implies that potentially chemical or other influence of CO₂ sorption, such as reduction of breakdown pressures, is reducing the strength as it is known that carbon dioxide dissolves in coal enabling physical structure rearrangements (e.g. Larsen, 2004). In particular, residual strengths are up to 32% and 62% lower than the effective compressive strengths for samples saturated at 2.1 MPa and 4.3 MPa, respectively. Hence, the effect of CO₂ sorption on the structural rearrangement increases with saturation pressure within the subcritical region. However, further inspection of Fig. 8 shows that residual strengths of coals saturated at 8.5 MPa are higher than effective compressive strengths. Therefore, it can be inferred that the maximum alteration of the coal structure due to CO₂ adsorption was achieved at 4.3 MPa and that increasing the saturation pressure from subcritical CO₂ to its supercritical state had negligible impact on further reduction of strength. As previously mentioned, the results are contrary to the findings suggested in the literature that CO₂ phase transition from subcritical to supercritical state results in 40% and 46 % greater

strength reduction for bituminous and brown coals, respectively (e.g. Perera et al. 2013; Ranathunga et al., 2016a).

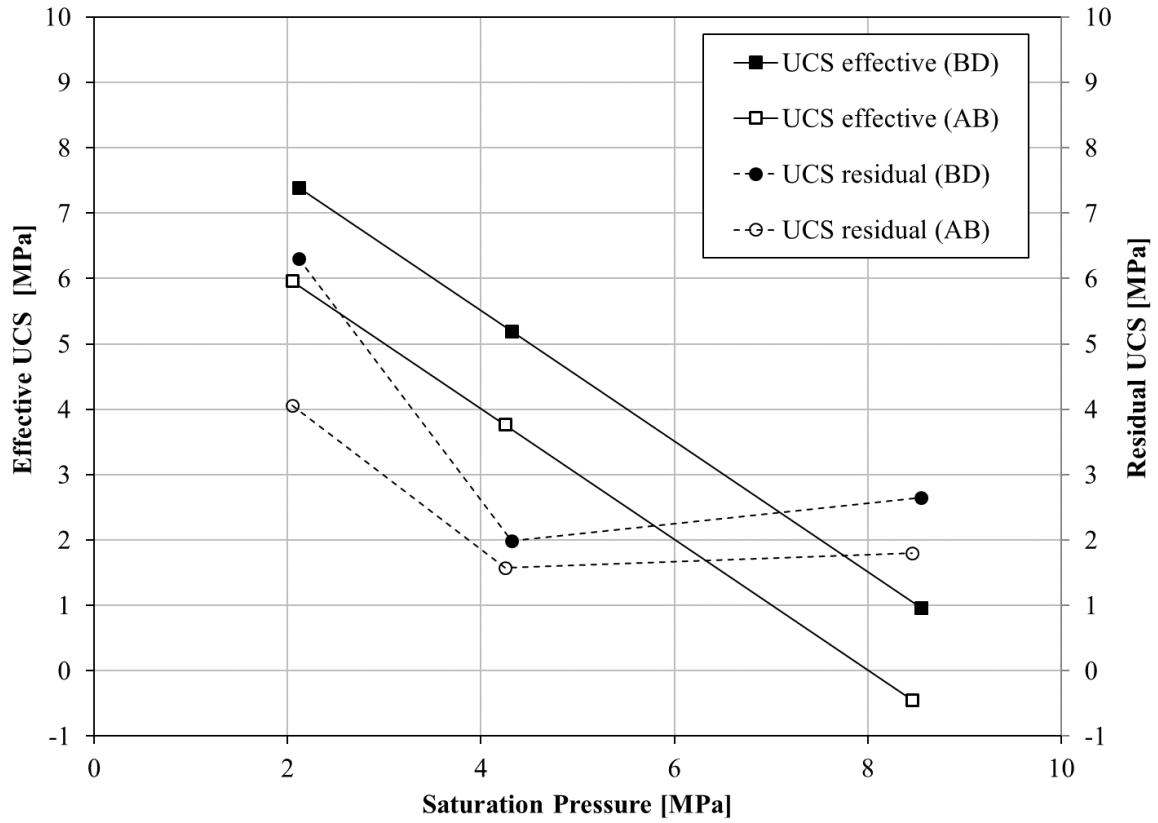


Fig. 8. Comparison between the Effective UCS and Residual UCS with respect to CO₂ saturation pressure.

3.1. Parametrisation of changes in UCS and E

The observed reductions in elastic modulus and unconfined compressive strength values are quantified by fitting a simple model to the experimental results and obtaining the fitting parameters. Since the change in measured parameters is caused by gas sorption, such change can be mathematically related to gas pressure (Masoudian et al., 2014).

Following the approach that the elastic modulus reduction is most commonly modelled using a Langmuir (1918) equation, ΔE can be written as (Masoudian et al., 2014):

$$\Delta E = \Delta E_{max} \frac{P}{P_E + P} \quad (3)$$

where ΔE_{max} is the maximum reduction in elastic modulus (Langmuir parameter), P is the gas pressure (MPa) and P_E is the Langmuir pressure (MPa) of elastic modulus reduction.

Similarly, ΔUCS can be written as (Masoudian et al., 2014):

$$\Delta UCS = \Delta UCS_{max} \frac{P}{P_{UCS} + P} \quad (4)$$

where ΔUCS_{max} is the maximum reduction in strength (Langmuir parameter) and P_{UCS} is the Langmuir pressure (MPa) of unconfined compressive strength reduction.

The fitting of the Langmuir curve to the experimental data was conducted using the sum of the squared differences with a target function which was minimized with respect to the Langmuir parameters using the Excel solver function.

Fig. 9 and Fig. 10 present the curves fitted to the experimental data of unconfined compressive strength and elastic modulus reductions of both samples as a function of CO₂ pressure, respectively. The parameters obtained using the fitting approach related to the reduction of deformation parameters of both coals are shown in Table 5. The unconfined compressive strength and elastic modulus of CO₂ saturated AB coal experience half of their maximum reduction at 1.69 MPa and 1.53 MPa gas pressures, respectively. In comparison, BD experienced half of the maximum reduction of unconfined compressive strength and elastic modulus at 2.53 MPa and 2.74 MPa, respectively.

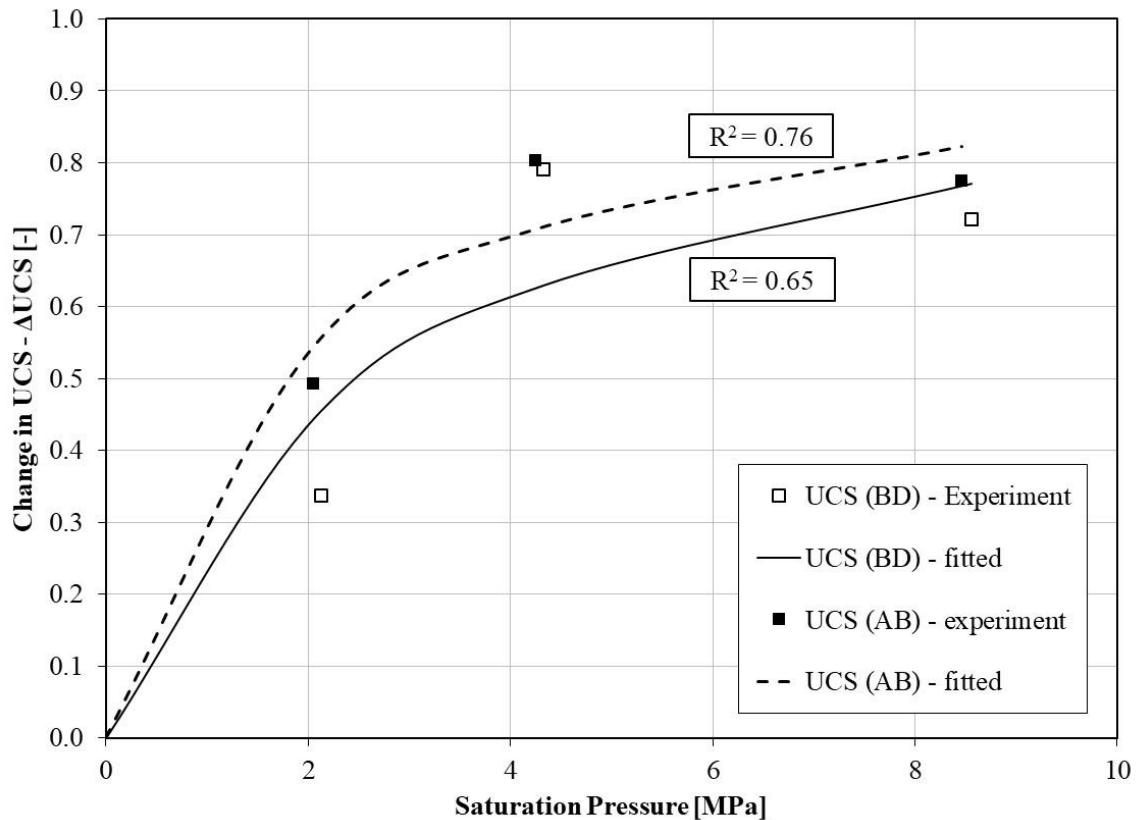


Fig. 9. The unconfined compressive strength reduction isotherms fitted to the calculated unconfined compressive strength reduction values of BD and AB coals.

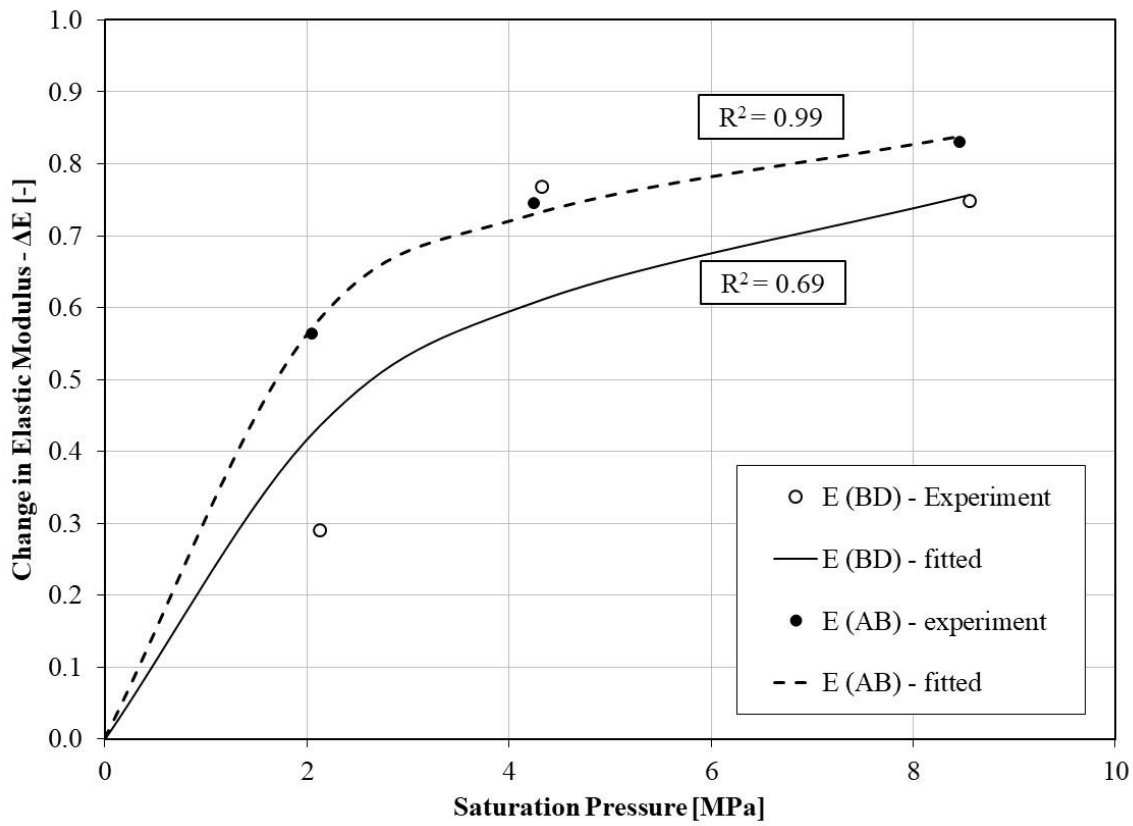


Fig. 10. The elastic modulus reduction isotherms fitted to the calculated elastic modulus reduction values of BD and AB coals.

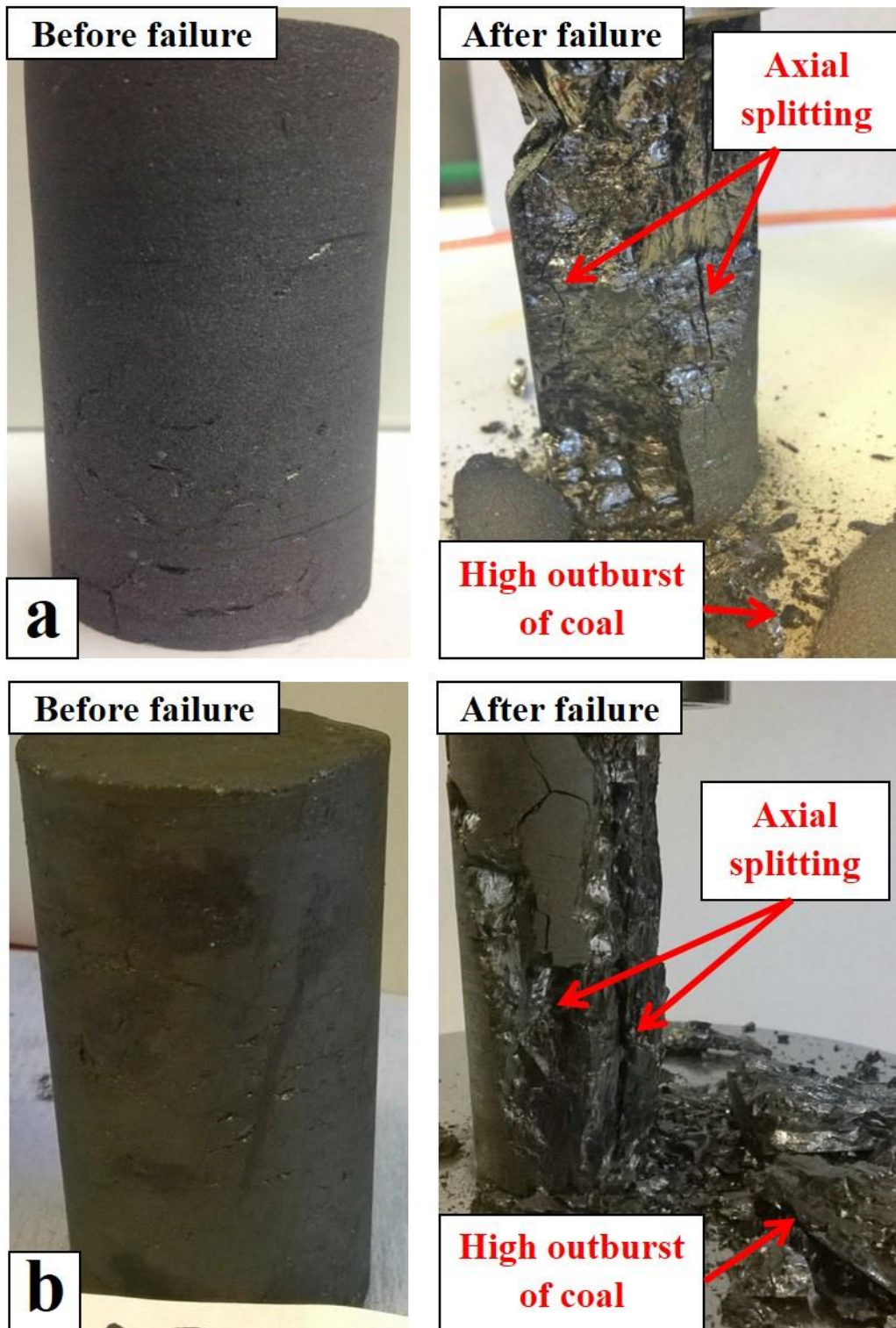
Table 5.

Fitted parameters of the proposed model for reduction of unconfined compressive strength and elastic modulus of BD and AB coals.

Deformation parameter	Fitted (Langmuir) parameters	
	P_{UCS} (MPa), P_E (MPa)	UCS_{max} (-), E_{max} (-)
Black Diamond		
Unconfined compressive strength	2.53	1.0
Elastic modulus	2.74	1.0
9ft Aberpergwm		
Unconfined compressive strength	1.69	0.98
Elastic modulus	1.53	0.99

3.2. Failure patterns

To visualize the effect of CO₂ saturation on failure mechanism of the coals considered in this study, photographs were taken before and after the failure of both natural and CO₂ saturated specimens. The photographs containing natural (non-saturated) samples and samples saturated at 2.1 MPa, 4.3 MPa and 8.5 MPa are shown in Fig. 11, 12, 13 and 14, respectively.



364

365 **Fig. 11.** Failure patterns of non-saturated coal samples; A) Black Diamond, B) 9ft Aberpergwm.

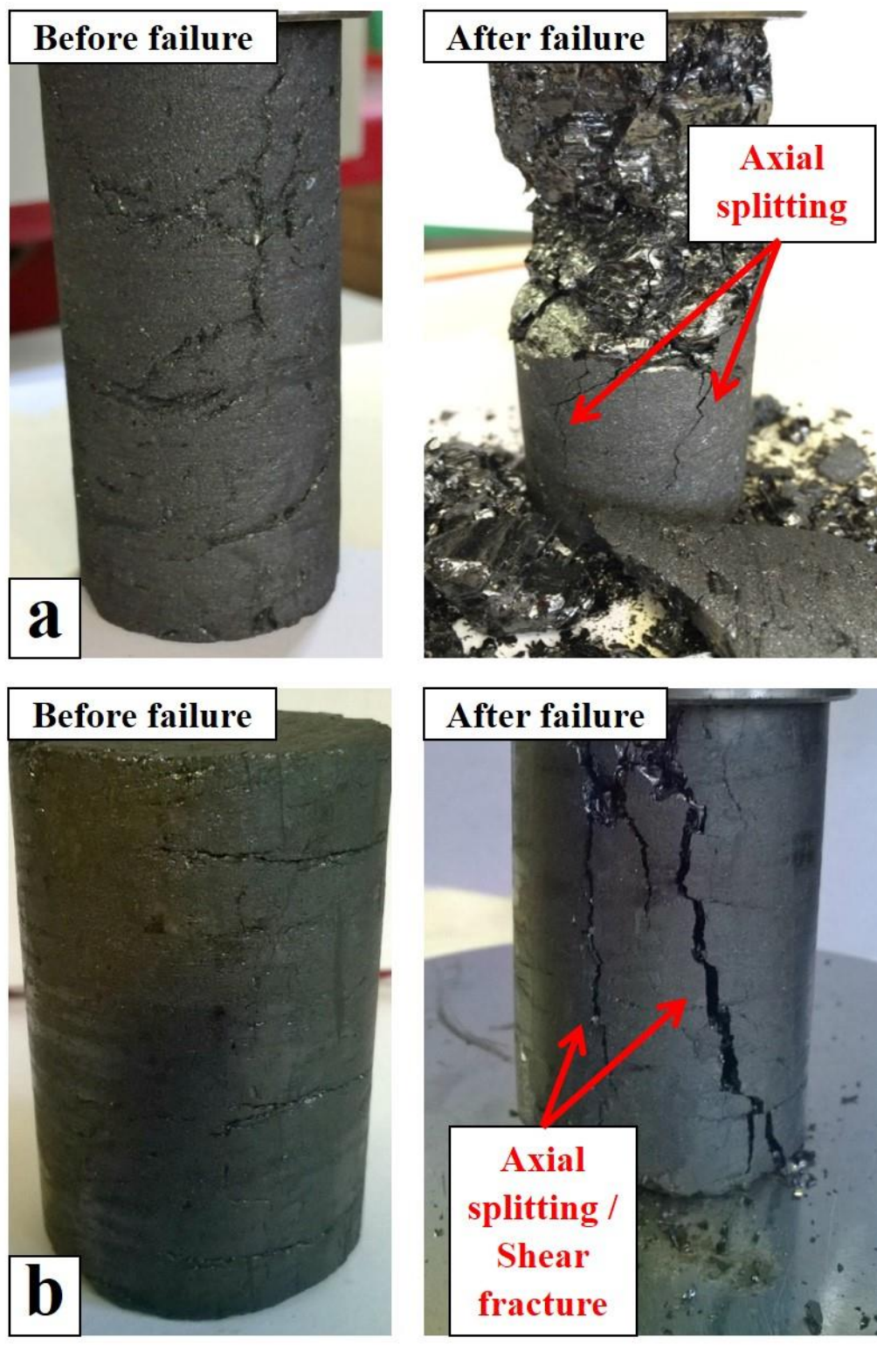


Fig. 12. Failure patterns of samples saturated with CO₂ at 2.1 MPa; A) Black Diamond, B) 9ft Aberpergwm.



Fig. 13. Failure patterns of samples saturated with CO₂ at 4.3 MPa; A) Black Diamond, B) 9ft Aberpergwm.

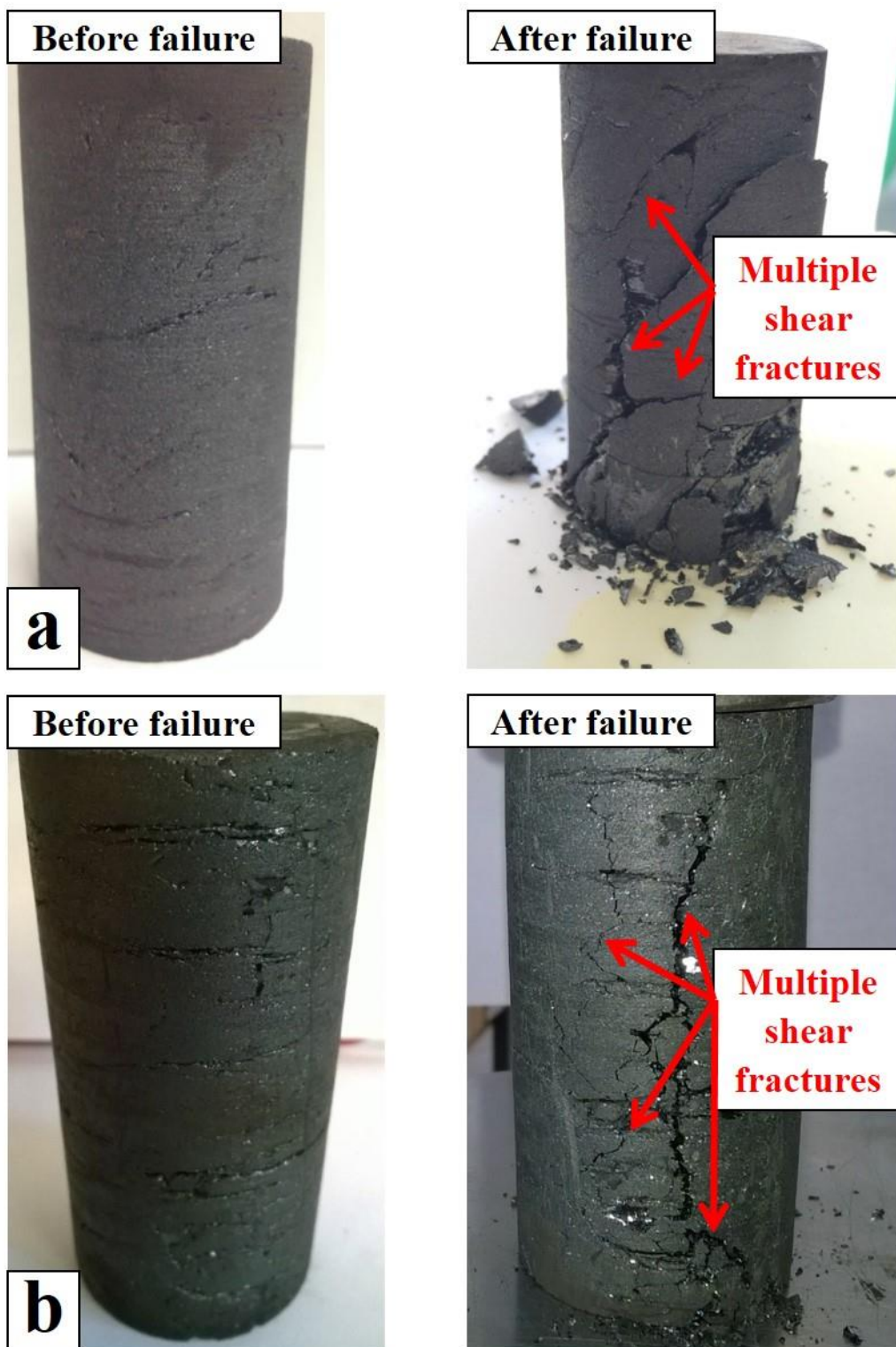


Fig. 14. Failure patterns of samples saturated with CO₂ at 8.5 MPa; A) Black Diamond, B) 9ft Aberpergwm.

Non-saturated coal samples failed predominantly through axial splitting where a number of axial cracks propagated along the entire length of the specimens (Fig. 11). Such splitting

occurred with rapid and unstable crack initiation and propagation, common for brittle materials, outbursting the samples into pieces.

Samples saturated with CO₂ at 2.1 MPa showed similar behaviour to those of non-saturated samples (Fig. 12). However, a set of non-longitudinal fractures was also visible, especially on the AB sample. Predominant shear failure occurred in samples saturated at 4.3 MPa of CO₂ (Fig. 13). In addition, a set of axial fractures was visible for both samples suggesting that the overall failure could be a combination of fracture propagation in axial and non-axial directions. For coals saturated in supercritical CO₂, i.e. at 8.5 MPa, multiple shear fractures orientated in different directions occurred with negligible material outburst during failure (Fig. 14).

Interestingly, both BD and AB samples showed comparable behaviour in terms of failure patterns. The only distinction is for specimens saturated at 2.1 MPa where BD exhibited higher outburst of the material than the AB coal showing predominantly axial splitting within the BD coal. This is in accordance with the strength parameter reduction (Fig. 7) where it is shown that AB samples saturated at 2.1 MPa lost more than half of their original strength while BD samples lost a third of their original strength. Consequently, higher residual strength of the BD coal could have resulted in a behaviour more similar to the natural, non-saturated samples.

Overall, by comparing failure types of non-saturated and CO₂ saturated specimens, a distinction can be observed. While former ones show predominantly axial splitting, the latter ones fail through a visible shear plane and existing fractures weakened by the CO₂ sorption. In unconfined compressive tests, irregular longitudinal splitting is the most common failure mechanism observed leading to an abrupt failure (Jaeger et al. 2007). Where the rock is fully ductile, a network of shear fractures will develop accompanied by plastic deformation of individual grains (Jaeger et al. 2007).

3.3. Post-failure sieve analysis

To assess the impact of CO₂ sorption on coal structure over the range of pressures used in this study, a post-failure sieve analysis of ten BD coal specimens was conducted. Fig. 15 shows coal particles as a result of a failure of both non-saturated and CO₂ saturated BD samples under axial compression. The failure of the non-saturated sample resulted in a large coal lump accompanied by a number of smaller particles. Conversely, CO₂ saturated samples show more gradual distribution of the coal particles.

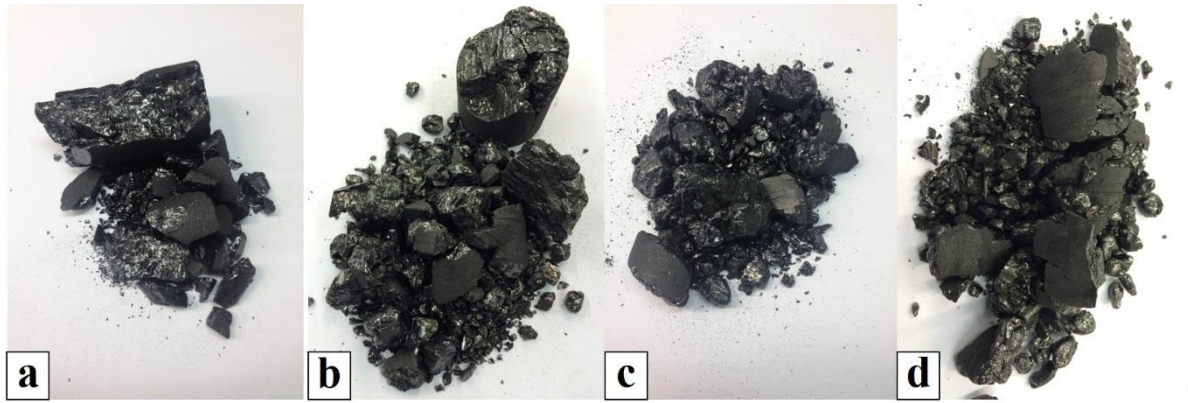


Fig. 15. Black Diamond coal post-failure particles; (a) natural (non-saturated) sample, (b) 2.1 MPa saturated sample; (c) 4.3 MPa saturated sample, (d) 8.5 MPa saturated sample.

Based on the results of the sieve analysis of ten BD specimens, the average percentage of particles passing through a certain sieve for natural and CO₂ saturated specimens was calculated. Comparison of the obtained average values with respect to sieve size is presented in Fig. 16.

Specimens saturated with CO₂ show higher percentage of particles passing through sieves than non-saturated specimens. On average, 7%, 15%, 28% and 30% of the total coal mass of non-saturated, 2.1 MPa saturated, 4.3 MPa saturated and 8.5 MPa saturated coal specimens passed through the largest sieve size of 6.3 mm, respectively. Such results confirm the previous assumption by Wang et al. (2011) that CO₂ saturated coals would result in smaller particles after the failure than the non-saturated specimens indirectly suggesting the micro-fracturing of the coal caused by CO₂ sorption. Additionally, it can be inferred from Fig. 16 that the percentage of particles passing through sieves depends on saturation pressure.

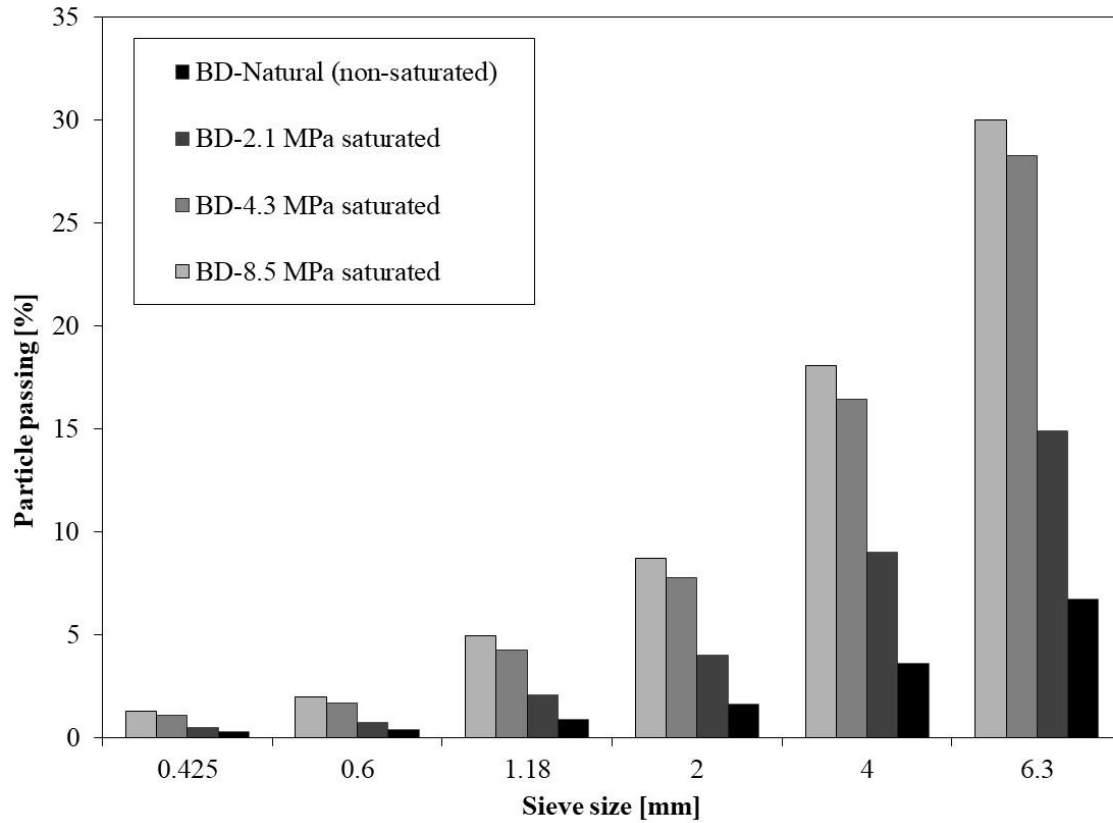


Fig. 16. Comparison of the post-failure particle size distribution of natural (non-saturated) and CO₂ saturated Black Diamond samples.

In order to assess the difference in percentages of particles passing through each sieve between the non-saturated and CO₂ saturated samples, Fig. 17 shows the passing ratio versus the gas saturation pressure for each sieve. Passing ratio is calculated as the average percentage of particles passing through an individual sieve for CO₂ saturated samples divided by the average percentage of particles passing for natural (non-saturated) coal specimens.

Fig. 17 shows that for specimens saturated at 2.1 MPa, there are 1.7 to 2.5 more particles passing through the sieves compared to non-saturated specimens. For specimens saturated at 4.3 MPa and 8.5 MPa, the amount of particles passing through all the sieves compared to non-saturated specimens is 3.9-4.9 and 4.5-5.6 times higher, respectively. Hence, as the saturation pressure increases, the passing ratio steeply increases up to 4.3 MPa and then shows a more gradual further increase with gas pressure.

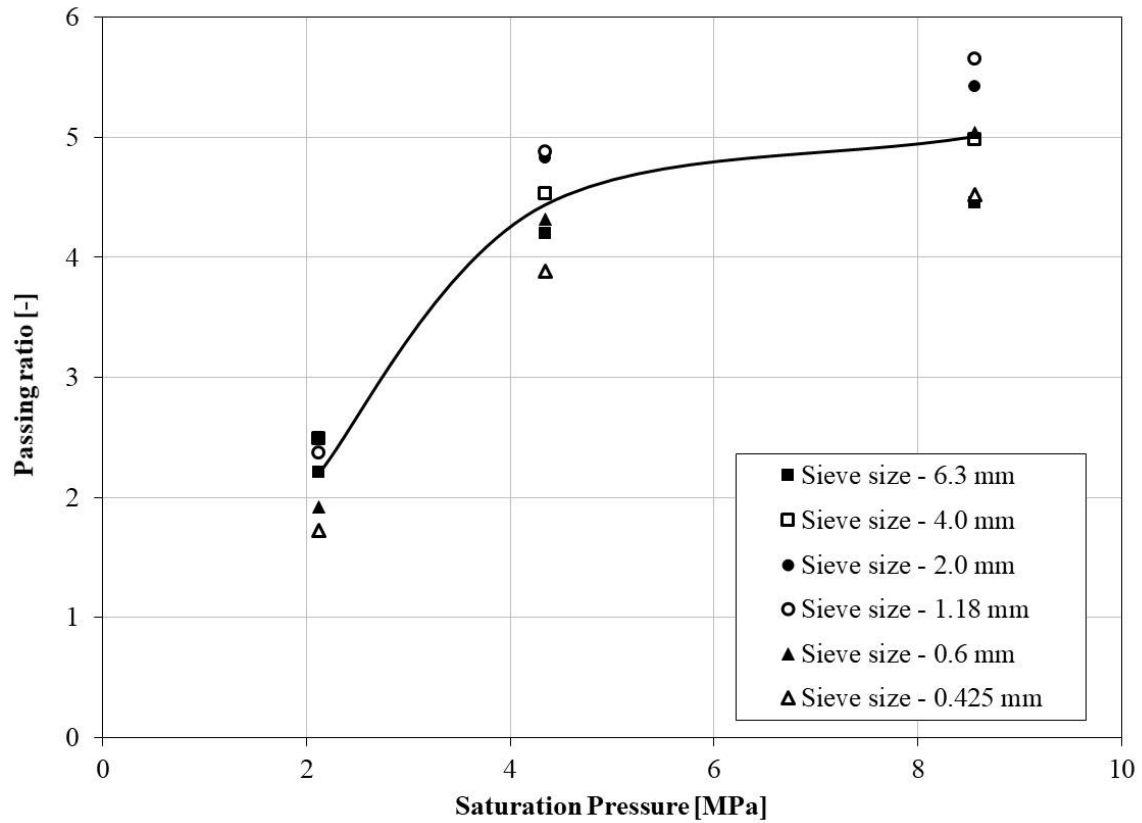


Fig. 17. Passing ratio versus the saturation pressure for particles passing through sieves of different sizes.

4. Discussion and Conclusions

The main aim of this study was to investigate the influence of sub- and supercritical CO₂ sorption on elastic deformation and failure of unconfined coal specimens subject to axial load. Two high rank coals collected from different locations of the South Wales Coalfield and from depths of 150 m (Black Diamond coal) and 550 m (Aberpergwm 9ft coal) were considered and in total, 20 samples were tested.

Based on the results of this study, unconfined compressive strengths and elastic moduli exhibit a linear relationship demonstrating that any loss in the elastic modulus is accompanied by the corresponding loss in the compressive strength of high rank coals.

The results also show that samples of both coals experience maximum reduction in elastic modulus and strength at 4.3 MPa, i.e. between 75% and 80%, where CO₂ is in the gaseous state. However, additional increase in CO₂ pressure to its supercritical state at 8.5 MPa had negligible effect on further reduction in measured parameters which was measured to be between 72% and 83%. Hence, this leads to the conclusion that the reduction of elastic modulus

and compressive strength of high rank coals is related to their sorptive behaviour. In other words, by achieving more than half of their maximum sorption capacity in the low pressure subcritical region, the corresponding structural rearrangement and consequent reduction in measured geomechanical parameters of high rank coals occurs in the same pressure region. This has been further confirmed by accommodating the effect of effective stress which suggested that chemical weakening of coal through its structural rearrangement occurs in the subcritical region and that there is a negligible further weakening effect due to the presence of supercritical CO₂ which is contrary to the findings previously reported in the literature for lignite and bituminous coals.

Although BD coal showed higher absolute values of unconfined compressive strengths and elastic moduli than the AB coal, the reduction percentage of deformation parameters of both samples is similar, especially at 4.3 MPa and 8.5 MPa saturation pressures. Hence, despite both anthracite coals considered in this study being from different locations and depths of the South Wales Coalfield, similar trends obtained on the samples of both coals suggest that geomechanical property alterations are rank related.

Visual inspection of the failure patterns showed that non-saturated specimens failed predominantly through axial splitting with high outburst of the material during compression, while the failure of the cores saturated with CO₂ occurred through a combination of shear fractures oriented in different directions with negligible material outburst common for ductile materials. Possible formation of micro fractures in the CO₂ saturated samples, previously suggested in the literature, was further confirmed by the results of the post-failure sieve analysis. The results showed that on average, only 7% of non-saturated particles passed through 6.3 mm sieve, while 2.1 MPa saturated, 4.3 MPa and 8.5 MPa saturated coals showed 15%, 28% and 30% of particles passing through the same sieve, respectively. Under those circumstances, it can be concluded due to the fact that CO₂ treated samples disintegrated on smaller particles than specimens without any CO₂ saturation after the failure, geomechanical property changes are a result of the weakened coal structure through the enhancement of the existing and inducement of new fractures.

Overall, this study demonstrated the weakening effect of CO₂ on high-rank anthracitic coals making them more ductile and less resistive to deformation under applied stress. Presented observations imply that the reduction of the coal deformation properties due to CO₂ sorption could contribute to the overall performance of a coal seam subject to CO₂ sequestration. On one hand, coal weakening could have a potentially negative impact on the structural integrity

of the CO₂ storage reservoir which could be eliminated by targeting coal seams with structurally sound overburden.

On the other hand, enhancement of existing fractures and creation of new ones could be a positive feature from the CO₂ injection standpoint as newly formed fractures could offer additional pathways for CO₂ flow and increase the amount of CO₂ injected in seams by offsetting the impact of coal swelling on CO₂ injectivity. Furthermore, reduction in elastic modulus of the target coals would result in increasing the fracture apertures under high pressure gas flow, again enabling easier access for the CO₂ molecules to the sorption sites. Based on the abovementioned, it can be implied that high rank coals could offer a good prospect of storing CO₂. Hence, future work will focus to enhance the current understanding of how the changes in deformation properties induced by CO₂ sorption affect the coal's transport and storage properties.

According to the author's knowledge, this is the first experimental analysis of anthracite coal's behaviour as well as the behaviour of South Wales coals dealing with the change in deformation properties of coals subject to sub- and supercritical CO₂ pressures up to 8.5 MPa.

5. Acknowledgements

This work was carried out as a part of SEREN and FLEXIS Projects. Both projects have been part-funded by the European Regional Development Fund through the Welsh Government. The financial support, for the first author, is gratefully acknowledged. The authors wish to express their appreciation to EnergyBuild Ltd, Walter Energy Inc. and Celtic Energy Ltd for providing coal blocks to conduct this research.

6. References

- ASTM Standards, 2012. *ASTM D2013. Standard practice of preparing coal samples for analysis. Vol. 05.06.* West Conshohocken, PA: ASTM International.
- ASTM Standards, 2014. *ASTM D7012. Standard Test Methods for Compressive Strength and Elastic Moduli of Intact Rock Core Specimens under Varying States of Stress and Temperatures. Vol. 04.09.* West Conshohocken, PA: ASTM International.
- ASTM Standards, 2015. *ASTM D388. Standard Classification of Coals by Rank. Vol. 05.06.* West Conshohocken, PA: ASTM International.
- ASTM Standards, 2015. *ASTM D3302/D3302M. Standard Test Method for Total Moisture in Coal. Vol. 05.06.* West Conshohocken, PA: ASTM International.

523 British Standards Institution, 1990. *BS 1377-2:1990. Methods of test for soils for civil engineering*
524 *purposes. Clasification tests*. Milton Keynes: BSI.

525 British Standards Institution, 1996. *BS 1016-106.1.1:1996. Methods for analysis and testing of coal and*
526 *coke. Ultimate analysis of coal and coke. Determination of carbon and hydrogen content, high*
527 *temperature combustion method*. Milton Keynes: BSI.

528 British Standards Institution, 1996. *BS 1016-106.4.2:1996. Methods for analysis and testing of coal and*
529 *coke. Ultimate analysis of coal and coke. Determination of total sulfur content, high temperature*
530 *combustion method*. Milton Keynes: BSI.

531 British Standards Institution, 1998. *BS 1016-104.3:1998. Methods for analysis and testing of coal and*
532 *coke. Proximate analysis, determination of volatile matter content*. Milton Keynes: BSI.

533 British Standards Institution, 1998. *BS 1016-104.4:1998. Methods for analysis and testing of coal and*
534 *coke. Proximate analysis, determination of ash*. Milton Keynes: BSI.

535 British Standards Institution, 1999. *BS 1016-104.1:1999. Methods for analysing and testing of coal and*
536 *coke. Proximate analysis, determination of moisture content of the general analysis tests sample*. Milton
537 Keynes: BSI.

538 Busch, A. and Gensterblum, Y. 2011. CBM and CO₂-ECBM related sorption processes in coal: A
539 review. *International Journal of Coal Geology*, 87(2), pp. 49-71.

540 Gathitu, B.B., Chen, W.Y. and McClure, M. 2009. Effects of Coal Interaction with Supercritical CO₂:
541 Physical Structure. *Industrial & Engineering Chemistry Research*, 48(10), pp. 5024-5034.

542 Gensterblum, Y. 2013. *CBM and CO₂-ECBM related sorption processes in coal*. Ph.D. Thesis, RWTH
543 Aachen University, Germany.

544 Gensterblum, Y., van Hemert, P., Billemon, P., Battistutta, E., Busch, A., Krooss, B.M., De Weireld,
545 G. and Wolf, K.H.A.A. 2010. European inter-laboratory comparison of high pressure CO₂ sorption
546 isotherms II: Natural coals. *International Journal of Coal Geology*. 84(2), pp. 115-124.

547 Hol, S., Spiers, C.J. and Peach, C.J. 2012. Microfracturing of coal due to interaction with CO₂ under
548 unconfined conditions. *Fuel*, 97, pp. 569-584.

549 Hol, S., Gensterblum, Y. and Massarotto, P. 2014. Sorption and changes in bulk modulus of coal –
550 experimental evidence and governing mechanisms for CBM and ECBM applications. *International*
551 *Journal of Coal Geology*, 128-129, pp. 119-133.

552 Jaeger, J.C., Cook, N.G.W. and Zimmerman, R.W. 2007. *Fundamentals of Rock Mechanics*, 4th Edition,
553 Blackwell Publishing.

554 Jones, N.S., Holloway, S., Smith, N.J.P., Browne, M.A.E., Creedy, D.P., Garner, K. and Durucan, S.
555 2004. *UK Coal Resource for New Exploitation Technologies*. DTI Report No. COAL R271, DTI/Pub
556 URN 04/1879. DTI Cleaner Coal Technology Transfer Programme, Harwell.

557 Karacan, C.Ö. 2007. Swelling-induced volumetric strains internal to a stressed coal associated with CO₂
558 sorption. *International Journal of Coal Geology*, 72(3-4), pp. 209-220.

559 Langmuir, I. 1918. The adsorption of gases on plane surfaces of glass, mica and platinum. *Journal of*
560 *the American Chemical Society*, 40(9), pp. 1361-1403.

561 Larsen, J.W. 2004. The effects of dissolved CO₂ on coal structure and properties. *International Journal*
562 *of Coal Geology*, 57, pp. 63-70.

563 Li, D., Liu, Q., Weniger, P., Gensterblum, Y., Busch, A. and Krooss, B.M. 2010. High-pressure sorption
564 isotherms and sorption kinetics of CH₄ and CO₂ on coals. *Fuel*, 89(3), pp. 569-580.

565 Liu, C.J., Wang, G.X., Sang, S.X. and Rudolph, V. 2010. Changes in pore structure of anthracite coal
566 associated with CO₂ sequestration process. *Fuel*, 89(10), pp. 2665-2672.

567 Liu, C.J., Wang, G.X., Sang, S.X., Gilani, W. and Rudolph V. 2015. Fractal analysis in pore structure
568 of coal under conditions of CO₂ sequestration process. *Fuel*, 139, pp. 125-132.

569 Masoudian, M.S., Airey, D.W. and El-Zein, A. 2014. Experimental investigations on the effect of CO₂
570 on mechanics of coal. *International Journal of Coal Geology*, 128-129, pp. 12-23.

571 Perera, M.S.A., Ranjith, P.G. and Peter, M. 2011. Effects of saturation medium and pressure on strength
572 parameters of Latrobe Valley brown coal: Carbon dioxide, water and nitrogen saturations. *Energy*,
573 36(12), pp. 6941-6947.

574 Perera, M.S.A., Ranjith, P.G. and Viete, D.R. 2013. Effects of gaseous and super-critical carbon dioxide
575 saturation on the mechanical properties of bituminous coal from the Southern Sydney Basin. *Applied*
576 *Energy*, 110, pp. 73-81.

577 Ranathunga, A.S., Perera, M.S.A., Ranjith, P.G. and Bui, H. 2016a. Super-critical CO₂ saturation-
578 induced property alterations in low rank coal: An experimental study. *The Journal of Supercritical*
579 *Fluids*, 109, pp. 134-140.

580 Ranathunga, A.S., Perera, M.S.A. and Ranjith P.G. 2016b. Influence of CO₂ adsorption on the strength
581 and elastic modulus of low rank Australian coal under confining pressure. *International Journal of Coal*
582 *Geology*, 167, pp. 148-156.

583 Ranjith, P.G. and Perera, M.S.A. 2012. Effects of cleat performance on strength reduction of coal in
584 CO₂ sequestration. *Energy*, 45(1), pp. 1069-1075.

585 Siemons, N. and Busch, A. 2007. Measurement and interpretation of supercritical CO₂ sorption on
586 various coals. *International Journal of Coal Geology*, 69(4), pp. 229-242.

587 Viete, D.R. and Ranjith, P.G. 2006. The effect of CO₂ on the geomechanical and permeability behaviour
588 of brown coal: Implications for coal seam CO₂ sequestration. *International Journal of Coal Geology*,
589 66, pp. 201-216.

590 Vishal, V., Ranjith, P.G. and Singh, T.N. 2015. An experimental investigation on behaviour of coal
591 under fluid saturation, using acoustic emission. *Journal of Natural Gas Science and Engineering*. 22,
592 pp. 428-436.

593 Wang, S., Elsworth, D. and Liu, J. 2011. Permeability evolution in fracture coal: the roles of fracture
594 geometry and water-content. *International Journal of Coal Geology*, 87(1), pp. 13-25.

595 Wang, S., Elsworth, D. and Liu, J. 2013. Mechanical Behavior of Methane Infiltrated Coal: the Roles
596 of Gas Desorption, Stress Level and Loading Rate. *Rock Mechanics and Rock Engineering*, 46, pp. 945-
597 958.

598 White, C.M., Smith, D.H., Jones, K.L., Goodman, A.L., Jikich, S.A., Lacount, R.B., Dubose, S.B.,
599 Ozdemir, E., Morsi, B., Schroeder, K.T. 2005. Sequestration of Carbon Dioxide in Coal with Enhanced
600 Coalbed Methane Recovery – A Review. *Energy&Fuels*, 19 (3), 659-724.

601 Zagorščak, R. 2017. *An Investigation of Coupled Processes in Coal in Response to High Pressure Gas*
602 *Injection*. Ph.D. Thesis, Cardiff University, Wales, UK.

603

604